

# AnyPlace: Learning Generalized Object Placement for Robot Manipulation

Yuchi Zhao<sup>1,2</sup>, Mirosław Bogdanovic<sup>1,2</sup>, Chengyuan Luo<sup>3</sup>, Steven Tohme<sup>4</sup>, Kourosh Darvish<sup>1,5</sup>  
 Alán Aspuru-Guzik<sup>1,2,5</sup>, Florian Shkurti<sup>1,2</sup>, Animesh Garg<sup>6</sup>

<sup>1</sup>University of Toronto <sup>2</sup>Vector Institute <sup>3</sup>Shanghai Jiao Tong University  
<sup>4</sup>Wilfrid Laurier University <sup>5</sup>Acceleration Consortium <sup>6</sup>Georgia Institute of Technology  
 Email: {allan.zhao, mirosław.bogdanovic}@utoronto.ca

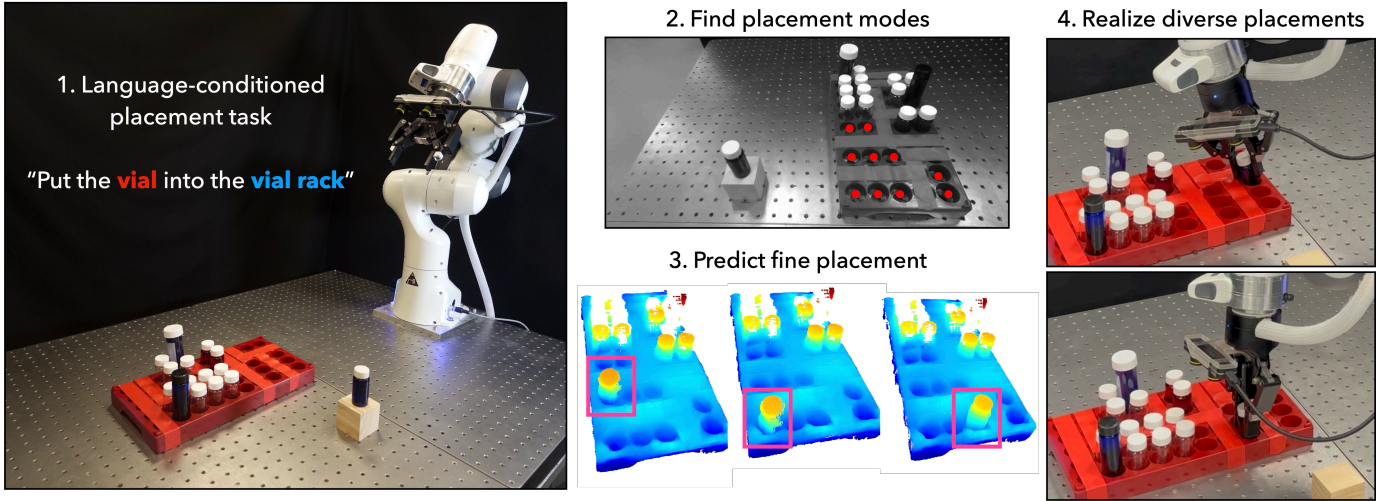


Fig. 1: Execution of the AnyPlace approach by the robot. (1) Given a language description of a placement task, the robot first captures an RGBD image of the scene using its eye-in-hand camera. (2) A large segmentation model and a Vision Language Model (VLM) are then used to segment objects and suggest possible placement locations. (3) Multiple placement poses are predicted for objects around these suggested locations. (4) The robot is then able to insert a vial into different holes on the vial plate.

**Abstract**—Object placement in robotic tasks is inherently challenging due to the diversity of object geometries and placement configurations. To address this, we propose AnyPlace, a two-stage method trained entirely on synthetic data, capable of predicting a wide range of feasible placement poses for real-world tasks. Our key insight is that by leveraging a Vision-Language Model (VLM) to identify rough placement locations, we focus only on the relevant regions for local placement, which enables us to train the low-level placement-pose-prediction model to capture diverse placements efficiently. For training, we generate a fully synthetic dataset of randomly generated objects in different placement configurations (insertion, stacking, hanging) and train local placement-prediction models. We conduct extensive evaluations in simulation, demonstrating that our method outperforms baselines in terms of success rate, coverage of possible placement modes, and precision. In real-world experiments, we show how our approach directly transfers models trained purely on synthetic data to the real world, where it successfully performs placements in scenarios where other models struggle – such as with varying object geometries, diverse placement modes, and achieving high precision for fine placement. More at: [any-place.github.io](https://any-place.github.io).

## I. INTRODUCTION

Placing objects is a fundamental task that humans perform effortlessly in daily life, from setting items on a table to inserting cables into sockets. On the other hand, enabling a robot to perform such tasks can often be highly challenging. The challenges arise from the various constraints of different placement tasks and the difficulty of generalizing to unseen objects. Existing methods are often task-specific, using a large number of demonstrations for a single placement task, such as hanging objects on racks [28], with the hope that the robot can generalize to unseen objects. Alternatively, few-shot approaches focus on learning object placement with only a few demonstrations, aiming for the model to replicate the same placement operation across random initial configurations of similar objects and setups.

Learning diverse object placements presents significant challenges for existing models, primarily due to the difficulty of generalization. Generalization can be categorized into two aspects: object-level and task-level. Object-level generalization

focuses on developing robust representations of various objects and placement configurations, enabling the model to handle unseen objects effectively. Task-level generalization involves the model’s ability to predict diverse placement configurations from given pointclouds. Additionally, predicting multimodal placement outputs—encompassing a range of valid locations and modes—remains challenging, particularly when multiple feasible solutions exist. For instance, a robot inserts a vial into one of many empty slots on a vial plate. Existing methods [26, 3, 27, 21, 24, 23, 9, 6, 15, 14] often operate within a few-shot learning framework, where they learn specific placements involving two particular objects, resulting in poor generalization to different tasks and object types. In contrast, RPDiff [28] has trained separate models for three placing scenarios (e.g. cup on a rack, book on a shelf, can stacking) using a relatively larger dataset, demonstrating some level of in-class object-level generalization, but its generalization to new tasks has not been studied.

In this work, we address generalizable object placement that is robust to different objects and capable of predicting diverse placement poses across various tasks, similar to general-purpose object grasping methods. To achieve this, we have developed a fully synthetic dataset that contains 1,489 generated objects and captures three common placement configurations: inserting, stacking, and hanging. Based on this dataset, we develop a placement prediction pipeline that consists of a high-level placement position proposal module and a low-level placement pose prediction model. For the high-level module, we leverage a large segmentation model SAM-2 [22] to segment objects of interest and prompt the Molmo VLM [4] to propose all possible placement locations. Only the region around the proposed placement is fed into the low-level pose prediction model. By first providing a rough region for the low-level module to focus on, the model can effectively generalize across objects, learn their geometry, and capture diverse placement configurations. For the low-level pose prediction models, we build upon diffusion to predict precise and multimodal placement poses. We demonstrate the effectiveness of our methods across different placement tasks in simulation, where we significantly outperform baseline models in terms of pick-and-place success rate and placement location coverage. In real-world evaluation, our model achieves an 80% success rate on the vial insertion task, demonstrating robustness to noisy data and generalization to unseen objects.

To summarize, the key contributions of our work are:

- 1) We propose a novel object placement approach that leverages a VLM to reason about potential placement locations and a low-level pose prediction model to predict placement poses based solely on the region of interest.
- 2) We developed a fully synthetic dataset containing thousands of generated objects capturing a wide range of local placement configurations. This is crucial in enabling us to train models exclusively on synthetic data and be able to use them for a wide range of real-world placement tasks.

- 3) We show that reducing the problem to only local prediction allows us to improve performance with respect to baseline methods in terms of success rate, precision, and mode coverage. It also crucially makes it possible for a model trained on a fully synthetic dataset to show generalization that enables it to directly be deployed to the real world on a variety of placement tasks.

## II. RELATED WORK

### A. Object pick and place in robot manipulation

The problem of robot pick-and-place is typically formulated in two ways: object rearrangement and direct end-effector pose prediction. In object rearrangement, the goal is to train a model to predict the relative transformation of the object from its initial pose to its final placement pose. Assuming the grasping pose is generated by existing models, the final placing pose of the end-effector is calculated by multiplying the predicted relative transformation with the grasping pose. In this setting, many of the works focus on predicting explicit task-relevant features of both objects and then solving for the relative pose through optimization or regression. Specifically, the Neural Descriptor Fields (NDF) series of papers [26, 3, 27] learn the occupancy field of pointclouds as a representation. Then, a set of predefined keypoints attached to the placement object is used to interact with and query the occupancy feature field of the target object. By matching the queried features at each point to features collected during demonstrations, the optimal object transformation is determined. TaxPose [21] leverages transformer-based cross-attention to predict corresponding points between two objects and use differentiable singular value decomposition (SVD) to solve for the relative transformation. To guarantee the placement pose prediction model is robust to SE(3) transformations, i.e., SE(3)-equivariant, methods [24, 23, 9] explicitly predict perpoint type-0 and type-1 features for object point clouds and then solve an optimization problem to align these features into specific configurations based on demonstrations. All of these methods operate in a few-shot setting and can predict a single placement pose given two objects. It is crucial for models to capture and predict a distribution of placement poses, as not every placement pose is realizable by a robot due to its kinematic constraints. RPDiff [28], by contrast, trains a transformer with a diffusion mechanism on a large dataset, gradually denoising the object placement pose. However, their experiments reveal that the coverage of possible placement locations is incomplete. The fixed-size cropping mechanism used during diffusion may also struggle to generalize to objects of varying sizes. Additionally, a recent study [5] samples multiple stable placements in a simulation and employs a VLM to select the appropriate mode based on a language query. While these modes are discrete, each mode allows for the rotation of objects along their axis of symmetry, resulting in valid placement poses that form a continuous distribution.

An alternative approach to the pick-and-place task is predicting the robot’s end-effector pose directly. M2T2 [33], and Pick2Place [12] focus on planar object placement in



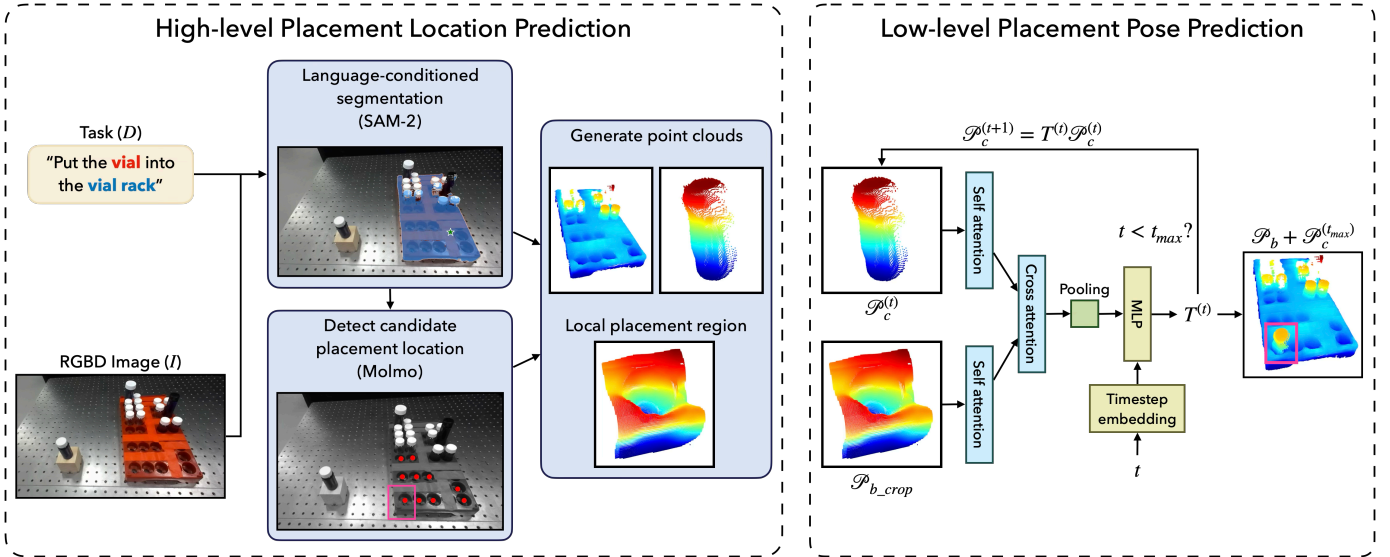


Fig. 2: **Overview of the AnyPlace placement pose prediction approach.** (1) High-level Placement Location Prediction: Given an input language description and an RGBD image, we leverage a VLM and a segmentation model to extract objects of interest. Next, we prompt the VLM again to propose possible placement locations. Using camera parameters, we reproject the depth map into 3D and crop the region of interest centered on the proposed placement location. Full pointclouds of the objects to be placed, along with the cropped regions of the placement locations, are then fed into our low-level pose prediction model to output precise relative transformations for object placement. (2) Low-level Placement Pose Prediction: We use self-attention to extract pointcloud features and cross-attention to capture cross-object features. For the diffusion decoder, the diffusion timestep is encoded within the MLP layers before the model outputs the relative transformation.

cluttered scenes. M2T2 [33] employs a multi-task transformer with separate decoders to predict grasp poses and placement location affordance maps for each discrete bin of rotation. Other works, like Pick2Place [12], concentrate on predicting key end-effector poses to accomplish specific tasks. RVT [10] and RVT-2 [11] also utilizes a transformer, leveraging multiview RGB images of the scene to predict heatmaps for the robot’s next end-effector location. Coarse-to-fine Q-attention [16], on the other hand, leverages the scene’s voxel to identify the most interesting spatial point at the current resolution. This point becomes the voxel centroid for the next refinement step, enabling the model to gather more accurate 3D information.

### B. Multimodal prediction in robot manipulation

Consider a mug that can be hung on a rack in various poses at different pegs. Multimodality of placement poses is common in manipulation. Recently advancements in behavior cloning methods, such as the IBC energy-based model [8] and Diffusion Policy [2], have attempted to capture this multimodality. For diffusion policy specifically, it learns to denoise action trajectories starting from a random noise distribution, enabling the model to capture the underlying distribution of possible solutions. Another approach to modeling these distributions is through Variational Autoencoders (VAEs). BeT [25] and VQ-Bet [17], for instance, trained a VQ-VAE [30] to discretize and encode continuous actions into latent representations, making it easier to handle multimodal and high-dimensional behavior data. To train the entire policy based on image

input, they employed a transformer-based model alongside the VAE decoder to predict sequences of actions. The authors demonstrated that their approach outperformed the Diffusion Policy [2] on common benchmarks.

### III. ANYPLACE: GENERALIZED OBJECT PLACEMENT

To enable a robot to execute diverse object placements in a scene, we propose breaking the placement pose prediction problem into two subtasks: a high-level placement location proposal task and a low-level fine-grained placement pose prediction task. For the high-level task, we incorporate a vision-language model, trained to output 2D keypoint locations in an image based on a given text prompt. A small local region around the candidate placement location can then be extracted and forwarded to the low-level pose-prediction model. This simplifies the low-level pose-prediction problem significantly by having a much smaller pointcloud as input and helps with generalization as any features outside of the local region do not influence the prediction. This allows us to focus on a limited set of general placement types and utilize a fully synthetic dataset, but have the final model be effective in a broad range of real-world placement tasks.

**Problem setup.** We formulate the object placement task to predict relative transformations. Specifically, given an input tuple  $\{D, I\}$ , where  $D$  represents the language description of the placement task and  $I$  is an RGBD image of the scene, our goal is to predict a set of rigid transformations  $\{T_n\}_{n=1}^N \subset \text{SE}(3)$  that move the target object  $C$  from its

current position to all viable placement locations on the base object  $B$  that satisfy language conditioning  $D$ . Assuming the grasping poses  $T_{\text{grasp}}$  are provided by a grasp prediction model, the final end-effector pose  $T_{\text{place}}$  can be computed using the predicted relative transformation between the initial object pose and its final placement pose as  $T_{\text{place}} = T_n T_{\text{pick}}$ .

#### A. VLM-guided placement location prediction

When objects have multiple potential placement locations, existing models often struggle to capture all these discrete positions when trained in an end-to-end manner. To address this, we propose leveraging recent advancements in VLMs, which have demonstrated strong capabilities in localizing points and regions within images based on language descriptions, to directly identify placement locations. Specifically, given a language description of the placement task  $D$  and a RGBD image  $I$ , we aim to extract the pointcloud of the target object  $\mathcal{P}_c$  and a local region of interest of the base object  $\mathcal{P}_{b_{\text{crop}}}$ , where  $\mathcal{P}_c, \mathcal{P}_{b_{\text{crop}}} \in \mathbb{R}^{N \times 3}$ . We utilize Molmo [4] to detect all potential placement locations as keypoints in image space, such as specifying all positions where a vial can be inserted into a vial plate. This approach enables the low-level pose prediction model to focus on learning the different placement configurations of two objects and predicting the placement pose without needing to explicitly capture multiple placement locations.

First, we extract segmentation masks for the target object  $C$  and the base object  $B$ . To achieve this, we first query the VLM to get point locations in the image for each object, then pass those points to the segmentation model to get segmentation masks. This allows us to have complex language conditioning in our object selection (e.g., "blue vial", "vial rack in front of the scale", etc.). Next, we query the VLM again on the base object  $B$  to find all the discrete modes for the placement (Figure 3). For each identified point in the image, we extract the local region in the pointcloud and use that as input to our pose prediction model.

Empirically, we found that explicitly identifying placement modes, rather than relying on models to explore placements across the entire object, is more reliable and practical when handling diverse objects with multiple possible placement poses. Additionally, since our high-level module is built on a general-purpose VLM, the system can handle diverse placements and perform complex language conditioning. In particular, this enables us to have complex language conditioning in: (1) selecting which object to place; (2) selecting which object to place it onto; and (3) selecting where on that object to perform the placement. It also enables our method to function effectively even when the object being placed onto is large or difficult to segment. This is because the module always outputs a small local region around the potential placement location, regardless of the object's size.

#### B. Fine-grained placement pose prediction

Given pointclouds  $\mathcal{P}_c$  and  $\mathcal{P}_{b_{\text{crop}}}$  from the high-level module, the low-level pose prediction model only focuses on learn-

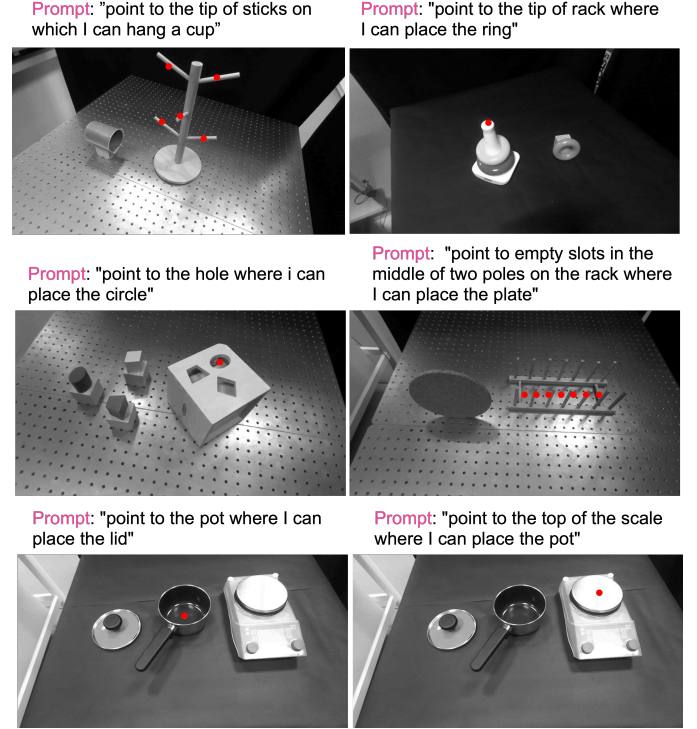


**Fig. 3: Language Prompts and VLM Output Visualization in the Real-World Evaluation.** In the real-world setting, we prompt the VLM to predict placement locations on a variety of different objects. Combined with our low-level pose prediction model, we demonstrate strong generalization and flexibility in real-world experiments. The red dot on each image is the predicted pixel location from the Molmo VLM.

ing different local placement arrangements, without the need to capture the distribution of different placement locations. Our intuition is that, with the aid of our large synthetic dataset, the model should effectively capture key representations of diverse placement configurations based on object geometry, which enables it to generalize to unseen objects and remain robust to noisy data. Having only a local region as input, the pose prediction model should be able to achieve better precision, which is crucial in many relevant placement tasks.

We predict the relative transformation in a diffusion process with a discrete number of timesteps. Starting with two object pointclouds, the diffusion process iteratively denoises the relative transformation, gradually moving the object being placed toward its final pose. Initially, we transform the object pointcloud  $\mathcal{P}_c$  with a random transformation  $T_{\text{init}} = (\mathbf{R}, \mathbf{t})$  to get  $\mathcal{P}_c^{(0)}$ , where  $\mathbf{R}$  is randomly sampled over the  $\text{SO}(3)$  space, and  $\mathbf{t}$  is sampled within the bounding box of the cropped placement region:

$$\mathcal{P}_c^{(0)} = T_{\text{init}} \mathcal{P}_c, \quad (1)$$

where

$$T_{\text{init}} = (\mathbf{R}, \mathbf{t}), \quad (2)$$

$$\mathbf{R} \sim \mathcal{U}(\text{SO}(3)), \quad \mathbf{t} \sim \mathcal{U}(\text{bbox}(\mathcal{P}_{b_{\text{crop}}}). \quad (3)$$

As shown in Figure 2, at each denoising timestep  $t$ ,  $\mathcal{P}_c^{(t)}$  and  $\mathcal{P}_{b\_crop}$  are input into the encoder. Specifically, both pointclouds are firstly downsampled to 1024 points using Farthest Point Sampling (FPS) and normalized to the size of a unit cube. The downsampled pointclouds are passed through a linear layer to extract latent features, which are subsequently concatenated with a one-hot vector used to identify the corresponding pointcloud. These combined features are then processed by the Transformer encoder [31, 1], where self-attention layers are applied to effectively extract features from the pointclouds. We then leverage cross-attention and pooling layers to further aggregate these features, producing a unified feature representation that captures the spatial relationship between the two objects. In the decoder, we first obtain the sinusoidal positional embedding of the diffusion timestep  $t$ . Finally, the joint pointcloud feature representation, along with the encoded timestep, is fed into MLP layers to predict the relative transformation  $T_n^{(t)}$  consisting of a rotation  $\mathbf{R} \in \text{SO}(3)$  and a translation  $\mathbf{t} \in \mathbb{R}^3$  for refining the object’s pose. The target object pointclouds are then transformed accordingly before proceeding to the next denoising step as  $\mathcal{P}_c^{(t-1)} = T_n^{(t)} \mathcal{P}_c^{(t)}$ . The full transformation  $T_n$  taking the object from its initial location to the placement pose is the product of all the incremental transformations predicted through the diffusion steps:  $T_n = \prod_{t=1}^{t_{\max}} T_n^{(t)}$ . More details on the model architecture can be found in the Appendix.

During training, we perform 5 denoising steps. Instead of incrementally adding Gaussian noise to the input during the forward process as is common practice [13], we manually define the noise added at each timestep. In our case, the noise is the relative transformation that the model predicts. Specifically, the intermediate ground truth relative transformations  $T_{n,GT}^{(t)}$  are generated by linearly interpolating the translation and using spherical linear interpolation (SLERP) to sample rotations between the object’s initial and final placement poses. During inference, we generate diverse placement poses by sampling the diffusion model multiple times, each time starting with randomly transformed initial object pointclouds  $\mathcal{P}_c^{(0)}$ . We perform a larger number of denoising steps at test time, by repeating the last denoising step more times for a total of 50 denoising steps.

At each diffusion step during training, given the ground truth  $T_{n,GT}^{(t)}$  and the predicted  $T_n^{(t)}$ , we use the L1 distance for the translation loss  $\mathcal{L}_{translation}$ . For rotation, we measure the geodesic distance between the ground truth and predicted rotations. Additionally, we apply Chamfer loss between the pointcloud transformed by the ground truth pose and by the predicted pose. The total loss is the summation of these losses:

$$\mathcal{L}_{total} = \mathcal{L}_{translation} + \mathcal{L}_{rotation} + \mathcal{L}_{chamfer} \quad (4)$$

### C. Robot pick and place execution

After determining the placement poses, we implement a pick-and-place pipeline to manipulate the object and position it accurately at the target pose. Specifically, we utilize AnyGrasp [7] to find viable grasps for the target object  $C$  and employ

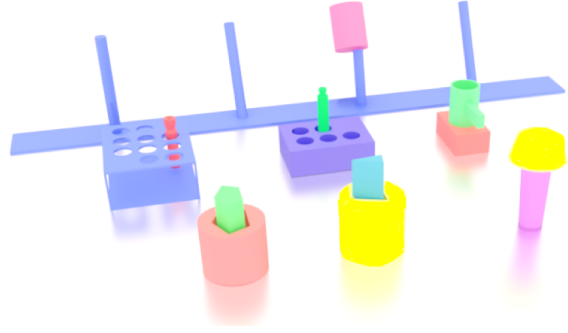


Fig. 4: **Generated objects in the synthetic dataset.** We use Blender to procedurally generate various categories of objects for three placement tasks: insertion, stacking, and hanging.

cuRobo [29] as the motion planner to perform collision-free placement. We perform rejection sampling on  $(T_{place}, T_{pick})$  pairs to identify valid grasps for the specific placement pose predicted by our model that can be executed by the robot.

Grasp detection begins by extracting the target object pointclouds  $\mathcal{P}_c$  from an RGBD image. AnyGrasp [7] then processes the resulting pointclouds to identify the optimal grasp candidates sorted by confidence. To pick up the object, the gripper is first moved to a pre-grasp pose, positioned 10 centimeters away from the target along the gripper’s z-axis. The gripper then approaches the target in a straight line while maintaining its orientation. Similarly, during placement, the robot first moves to a pre-place pose, followed by a final approach without altering the gripper orientation. The distance from the pre-place pose to the final placement pose is adjusted according to the object’s size to avoid collisions during the transition to the pre-place position. With the waypoints and end-effector orientation constraints defined, we use cuRobo to generate the complete motion plan for robot pick and place.

## IV. SYNTHETIC DATASET GENERATION

Our aim in building the synthetic dataset is to capture a broad range of local placement arrangements. Existing models use a few very specific tasks (e.g. inserting a book into a bookshelf) to simply evaluate how well their model works given placement data for such task for training [33, 12, 32].

Our goal on the other hand is not only to use the dataset to evaluate the proposed model, but to build towards representing a broad range of types of placements (stacking, hanging, inserting) as shown in Figure 4. The local nature of our pose-prediction model makes this task much easier and enables us to build a dataset that can generalize to a broad range of real-world placement tasks.

The data generation pipeline consists of two main components: object generation and placement pose generation. Specifically, we use Blender to procedurally generate 3D objects, such as pegs, holes, cups, racks, beakers, vials, and vial holders. Object parameters—including height, width, length, and number of edges—are randomized to increase variability. For racks and vial plates, we also randomize the number of



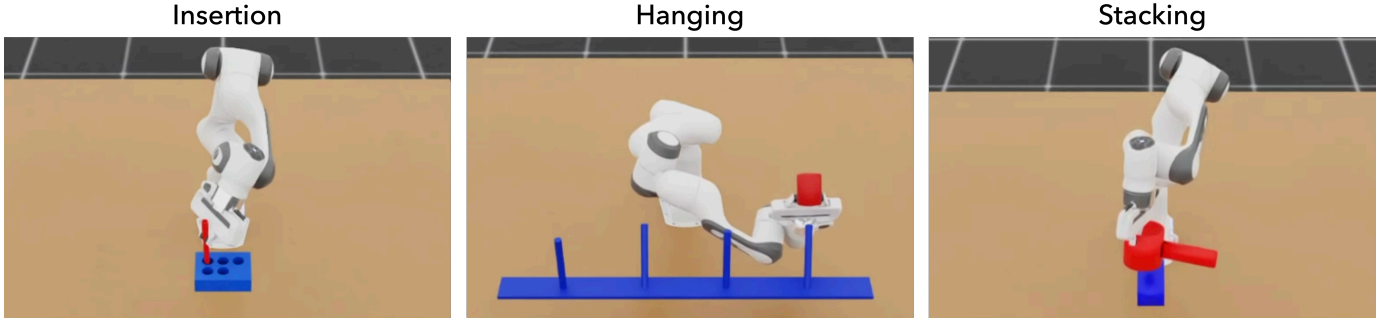


Fig. 5: **Robot performing various placement tasks in simulation.** In the simulation, given a set of predicted placement poses and grasping poses, we leverage cuRobo for motion planning and execute all trajectories simultaneously in IsaacLab.

poles and holes. Additionally, random scaling is applied along the x, y, and z axes to further enhance diversity.

To identify stable placements for objects, we use NVIDIA IsaacSim to determine object placement poses for three configurations: stacking, inserting, and hanging. At the start of each trial, two objects are randomly sampled and loaded into the simulation. Since all objects are procedurally generated and possible placement locations are known during generation (e.g., the center of each hole on a vial plate), the ideal object placement location for the placing object can easily be determined. This approach finds object placement locations that maximize the clearance between the objects in their final placement configurations. For object placement rotations, they are then randomly sampled along their axis of symmetry to explore various placement poses. Four cameras are set up to capture dense object pointclouds and render RGBD images. We believe that our dataset covers a wide range of placement scenarios encountered in real life. In total, 1489 objects across 13 categories were created, and 5370 placement poses were generated.

#### A. Training details

We train each model independently on subsets of the full dataset, split based on the type of placement configurations, as well as on the combined dataset (referred to as the “multitask” variant). While similar methods are typically trained for a single task (e.g., [28]), our goal is to build a single model capable of performing a diverse set of placement tasks. All single-task models are trained for three days, while multitask models are trained for five days on a single NVIDIA A100 GPU. More details on training parameters are in the Appendix.

### V. EXPERIMENTAL EVALUATION

We aim to evaluate three key aspects of our approach: success rate, coverage, and precision. With the VLM-based placement location prediction, our method effectively captures possible placement locations, achieving higher coverage rates. By narrowing the focus to minimal regions for placement pose prediction, we enable the model to achieve greater precision, which is essential for handling challenging placement tasks in real-world scenarios. All models are trained exclusively on

our synthetic dataset and evaluated on novel objects in a zero-shot setting. We conduct evaluations against three baseline models on different placement tasks in both simulation and real-world settings. Simulation enables extensive testing of our approach by leveraging rejection sampling across multiple parallel environments. In real-world experiments, we highlight the effectiveness and flexibility of our VLM-based placement location prediction in handling complex environments. Additionally, we demonstrate the robustness of our method in handling pointcloud noise and generalizing to unseen objects, despite being trained on general synthetic objects in simulation and encountering novel global configurations for similar types of local placements.

**Evaluation metrics.** We use three metrics to evaluate model performance: success rate, coverage, and precision. Specifically, we define a placement as successful if the robot places the object at the correct location and it remains stable after release. The success rate is then calculated as the number of successful placements divided by the total number of trials. To better understand the diversity of multimodal outputs in placement prediction, we evaluate coverage, defined as the number of distinct predicted placement locations relative to the total number of possible locations. Finally, for fine placement tasks, to evaluate the precision, we measure the error between the ground truth pose and the predicted pose in terms of both distance and angle.

**Baselines.** We compare our approach with three baselines: NSM [1], RPDiff [28], and an energy-based model (EBM) integrated with our high-level placement location prediction module. Specifically, NSM shares the same self-attention and cross-attention pointcloud encoder, paired with a simple regression decoder. For RPDiff, since the low-level pose-prediction module in our diffusion-based approach shares the same structure, this allows us to directly examine the effects of the high-level module we propose. We do not utilize a learned classifier on top of the pose prediction model that is present in RPDiff. Such a model can be applied on top of any of the methods we evaluate here, including the ones we propose. Not having it also allows us to evaluate the number of samples needed to achieve particular coverage of possible placement locations in the scene. To evaluate the effectiveness of the



TABLE I: **Success rate (%) on synthetic dataset.** We evaluate the baseline NSM, RPDiff, AnyPlace-EBM, and our method, AnyPlace, on the success rates of four pick-and-place tasks using objects from the synthetic dataset.

	Methods	Object Stacking (single-mode)	Peg Insertion (single-mode)	Cup Hang (multi-mode)	Vial Insertion (multi-mode)
<b>Single task training</b>	NSM	76.57	7.63	35.54	18.70
	RPDiff	<b>80.34</b>	22.94	92.02	16.51
	AnyPlace-EBM	<b>80.04</b>	8.44	91.57	65.64
	<b>AnyPlace</b>	<b>80.16</b>	<b>30.95</b>	<b>94.80</b>	<b>92.74</b>
<b>Multi-task training</b>	NSM	77.55	7.69	35.22	9.87
	RPDiff	<b>80.21</b>	22.33	<b>94.05</b>	24.26
	AnyPlace-EBM	78.95	10.75	90.87	57.24
	<b>AnyPlace</b>	78.28	<b>24.99</b>	<b>94.12</b>	<b>75.25</b>

diffusion decoder in generating multimodal outputs, we build an energy-based model, AnyPlace-EBM, for comparison. Inspired by Implicit-PDF [20], this model uses the same encoder as ours, but for the decoder, instead of explicitly predicting the placement pose, it includes two separate branches: one for placement location prediction and another for predicting the placement rotation energy. During training, we encourage all placement rotations in  $SO(3)$  that result in stable placements to have low energy. During inference, we randomly sample thousands of rotations and select the one with the lowest energy as the final placement rotation.

#### A. Placement Success: Single & Multi-Modal

For evaluating all the methods in simulation, we utilize the pick-and-place execution pipeline we constructed (subsection III-C), together with simulation in IsaacLab [19]. The pipeline itself can be used as a standalone module. It makes no assumptions about the placement prediction method and is not specifically tied to other modules in our approach. This enables it to be used as a general system for evaluating placement pose prediction models. In Figure 5 we show the system being used to perform insertion, hanging, and placement tasks. Combined with the synthetic dataset we create, this gives us a complete system for comparing different models and getting systematic results of success rate, mode coverage, and precision. Both motion planning and the pick-and-place simulation itself are GPU parallelizable, making evaluation of new models even easier.

We evaluate single-mode and multimodal placement across a set of 4 tasks. Object stacking and peg insertion tasks are Single-model placement since only one solution is feasible. While cup hang and vial insertion are multi-modal in nature due to the existence of multiple placement locations. We show a summary of placement experiments in these simulated domains in Table I.

We first examine single-mode tasks. For the simple stacking task, where high precision in placement poses is not required, AnyPlace and baseline models, including RPDiff and AnyPlace-EBM, achieve a similar success rate of around 80%. For the peg-in-hole task, which requires high precision

in placement pose prediction, AnyPlace surpasses the baseline models by a large margin.

Multi-mode tasks are where we expect to get full benefit from our approach. In the hanging task the tolerance for placing a cup on the rack is relatively high. AnyPlace achieves a 94% success rate in both single-task and multi-task settings, while RPDiff and AnyPlace-EBM perform slightly worse in comparison. Notably, NSM has the lowest success rate across all multi-mode tasks due to its inherent limitations as a regression model. In the more challenging vial insertion task, AnyPlace achieves the highest success rate of 92.74%, while the success rates of all baseline models drop significantly, with RPDiff reaching only 16.5%.

This demonstrates that relying on high-level VLM to propose possible placement locations and focusing solely on the local region for placement prediction, simplifies the task for low-level pose prediction models and enables them to better capture fine-grained pointcloud features for high-precision placements. Additionally, despite using the same high-level placement location prediction, the energy-based model suffers a performance drop of 27% and 18% in single-task and multi-task settings, respectively, compared to the diffusion-based AnyPlace. This highlights that the iterative denoising procedure in diffusion models is more effective for high-precision placement prediction.

#### B. Placement Coverage: Multi-Modal Insertion & Hanging

Now we aim to investigate how the coverage changes with the increase in the number of samples taken from each model. With how NSM and RPDiff are designed, we can only take independent samples from the model until as many possible placement modes are covered. In the case of AnyPlace and AnyPlace-EBM, the high-level VLM module predicts possible placement locations, so we can perform sampling for each mode. We perform an equal number of samples in each and compare performance for the same total number of samples for each model. All models used in this evaluation are trained on the multitask dataset.

In Figure 6 we show results for the vial insertion task. AnyPlace achieves close to its maximum performance after with a

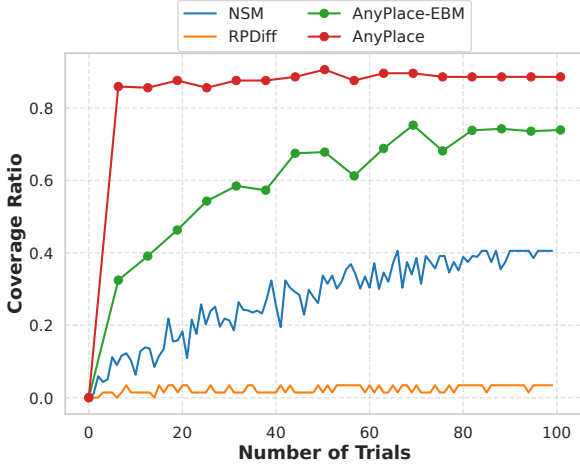


Fig. 6: **Comparison of vial insertion coverage across different models.** We show how the coverage ratio progresses with an increasing number of placement trials. AnyPlace clearly outperforms all baseline models as it rapidly reaches its maximum coverage.

single sample at each mode, outperforming other models with 100 samples. This is due to its high placement success rate and the VLM’s strong reasoning ability in identifying various possible placement locations. A similar trend is observed for the AnyPlace-EBM models; however, due to a lower placement success rate, the model plateaus at around 73%. In contrast, RPDiff, despite being a diffusion-based model that should capture multimodal outputs, fails in this regard, with coverage fluctuating below 10%. Even the NSM regression model outperforms it in this case, but still stays far below either of the methods utilizing the high-level VLM module.

For hanging, to further evaluate the effect of different objects on predicted placement coverage, we aim to assess how these models generalize to racks with different sizes, geometries, and spacing between the sticks. Specifically, we generate new racks with different physical parameters compared to those used during training. The success rates are shown in Table II, and the coverage is plotted in Figure 7. Similar to the vial insertion task, AnyPlace outperforms other baselines, consistently getting higher coverage with fewer samples and eventually reaching 100% coverage – made possible with the exceptional performance of the VLM module in finding the placement modes. RPDiff performs better in this case, but still struggles to cover all placement locations, with coverage saturating around 90%. This illustrates that the original RPDiff does not generalize well to objects with different geometries and sizes compared to the training set. In contrast, AnyPlace, aided by high-level placement prediction, allows the low-level prediction model to focus on learning placements based on local regions, thereby enabling strong generalization across varying object sizes and shapes.

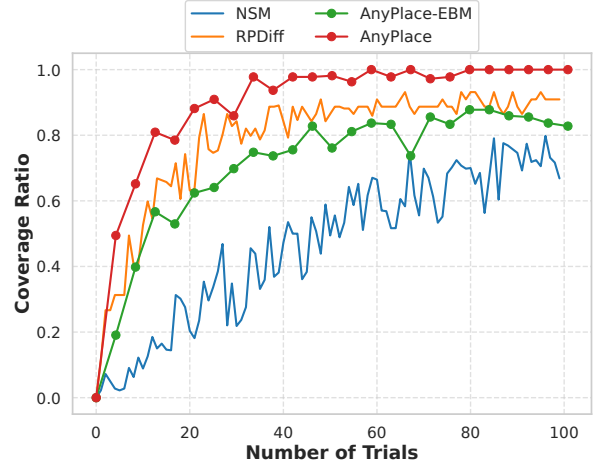


Fig. 7: **Comparison of hanging coverage across different models.** AnyPlace achieves nearly perfect coverage by leveraging the VLM’s ability to propose possible placement locations, whereas other baseline models fail to capture all placement modes.

### C. Placement Precision: Fine-Grained Insertion

The final evaluation we conduct in simulation focuses on assessing the precision of each approach. Precision is a critical factor in the successful completion of many placement tasks. Our goal is to determine whether providing models with a much smaller input region can enhance the precision of placement pose estimation. To achieve this, we evaluate the output of the prediction model directly rather than analyzing the results of the placement in simulation.

In Figure 8, we show the distribution of distance errors for each approach on the insertion tasks. Within model outputs that predict approximately the correct location, AnyPlace produces smaller errors and does so more reliably than the baselines. We also present the corresponding results for rotation prediction. Since the objects being placed are symmetric around the z-axis, we exclude yaw angle prediction from this comparison. As the initial pose is randomized and approaches cannot infer this orientation, all methods produce uniformly random yaw angle values. Given the minimal difference between the top and bottom sides of the object in this task, all approaches—except NSM, which performs the worst in both position and orientation—predict correct and flipped poses with roughly equal likelihood. Both AnyPlace and the RPDiff baseline perform well in predicting the correct orientation. Notably, the AnyPlace-EBM model achieves only slightly lower performance compared to the diffusion-based RPDiff and outperforms the NSM baseline. This is significant, as it highlights the potential of non-diffusion-based models for tackling these types of problems in future research.

### D. Real World Evaluation: Precise Multi-Modal Placement

We also evaluate the performance of our approach on various placement configurations with different objects in the real world. Specifically, for each scene, we capture a

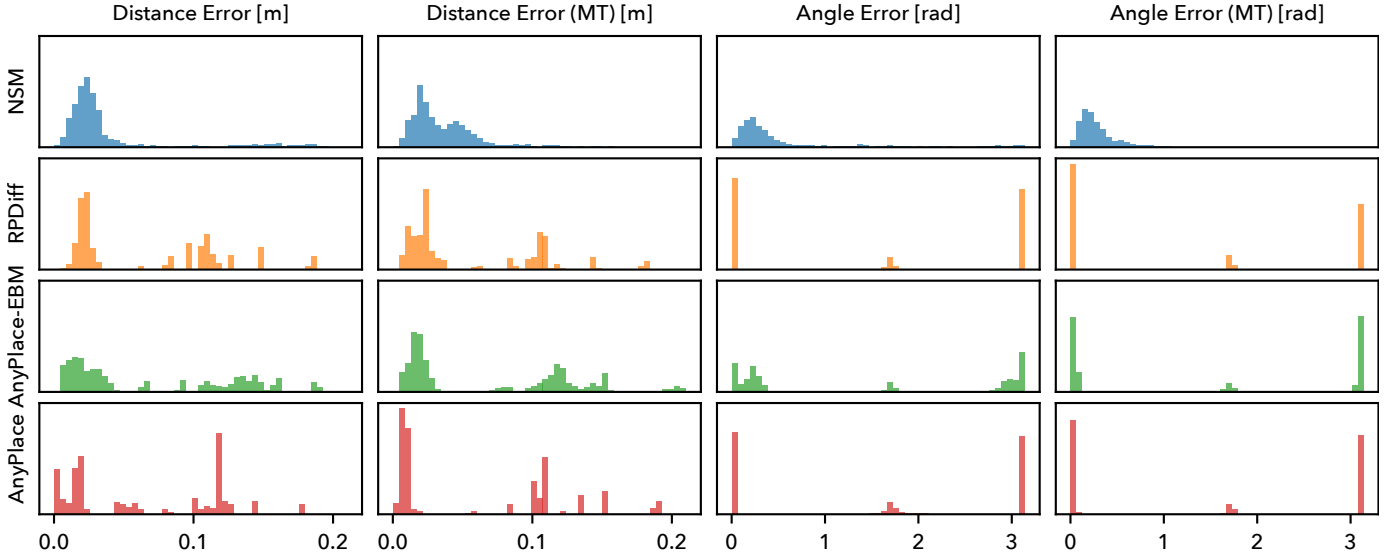


Fig. 8: **Distance and angle errors on insertion tasks.** We plot histograms of the translation and rotation error in pose prediction for each approach. We base the error on the position and rotation to the closest viable placement pose. (MT) denotes a model trained on multi-task data.

TABLE II: **Success rate of the hanging task across different models.** Using the evaluation procedure outlined in this section, we calculate the success rate of the hanging task on a rack with different object characteristics.

Methods	Success Rate
NSM Multitask	37.26%
RPDiff Multitask	81.17%
AnyPlace-EBM Multitask	69.43%
<b>AnyPlace Multitask</b>	<b>84.96%</b>

TABLE III: **Success rate of real robot executing vial insertion task.** Our model significantly outperforms baseline models in real experiments, demonstrating its ability to generalize to unseen objects and effectively handle noisy data.

Methods	Number of Success
NSM	0/10
RPDiff	0/10
AnyPlace-EBM	5/10
<b>AnyPlace</b>	<b>8/10</b>

single RGBD image with a ZED Mini camera mounted on a Franka Emika Robot arm. We use exactly the same high-level pipeline for detecting local placement locations as we do in our simulation experiments. We also utilize the same models, trained purely on our synthetic dataset, for predicting the placement poses in a zero-shot manner. We use a simplified pipeline for executing the placement, using a specific grasp and performing placement inverse kinematics instead of a full motion planner. In addition, we do not utilize rejection

sampling, but directly execute each trajectory on real. Our main goal is to evaluate whether enabling the model to predict only local placements would allow our models to generalize well to unseen objects in the real world even when only trained on our synthetic dataset. We perform systematic evaluations on the vial insertion task, with multiple possible placement locations. We also execute the approach on other language-conditioned placement variants in the real world, examples of which can be seen in Figure 9. All prompts used by the VLM to predict placement locations can be found in the Appendix.

We use a standard vial rack used in chemistry labs and randomly block different holes with other vials or cover them with tape to test the flexibility of our high-level placement location prediction module. Overall, across *10 trials*, the NSM and RPDiff fail to adapt to differences in this real-world task compared to the training conditions. AnyPlace, on the other hand, successfully completes placements, achieving the best performance, and inserts vials into 8 out of the 10 available empty spots in the vial rack.

#### E. Generalizable & Language-Conditioned Placement: Applicability in Real-World Tasks

To evaluate the generalization of AnyPlace, we conduct experiments on a large variety of objects for different placement configurations. As shown in Figure 9 (A), our method enables the robot to successfully perform placements in different scenarios, such as inserting a peg into a hole, hanging a cup on an unseen rack, and placing a plate into different slots of a plate rack. For precise placement, we demonstrate in Figure 9 (C) that the robot can accurately stack rings of varying radii, showcasing its ability to handle fine-grained placement tasks. Beyond single-step placements, AnyPlace excels in long-horizon tasks. For instance, we instruct the robot

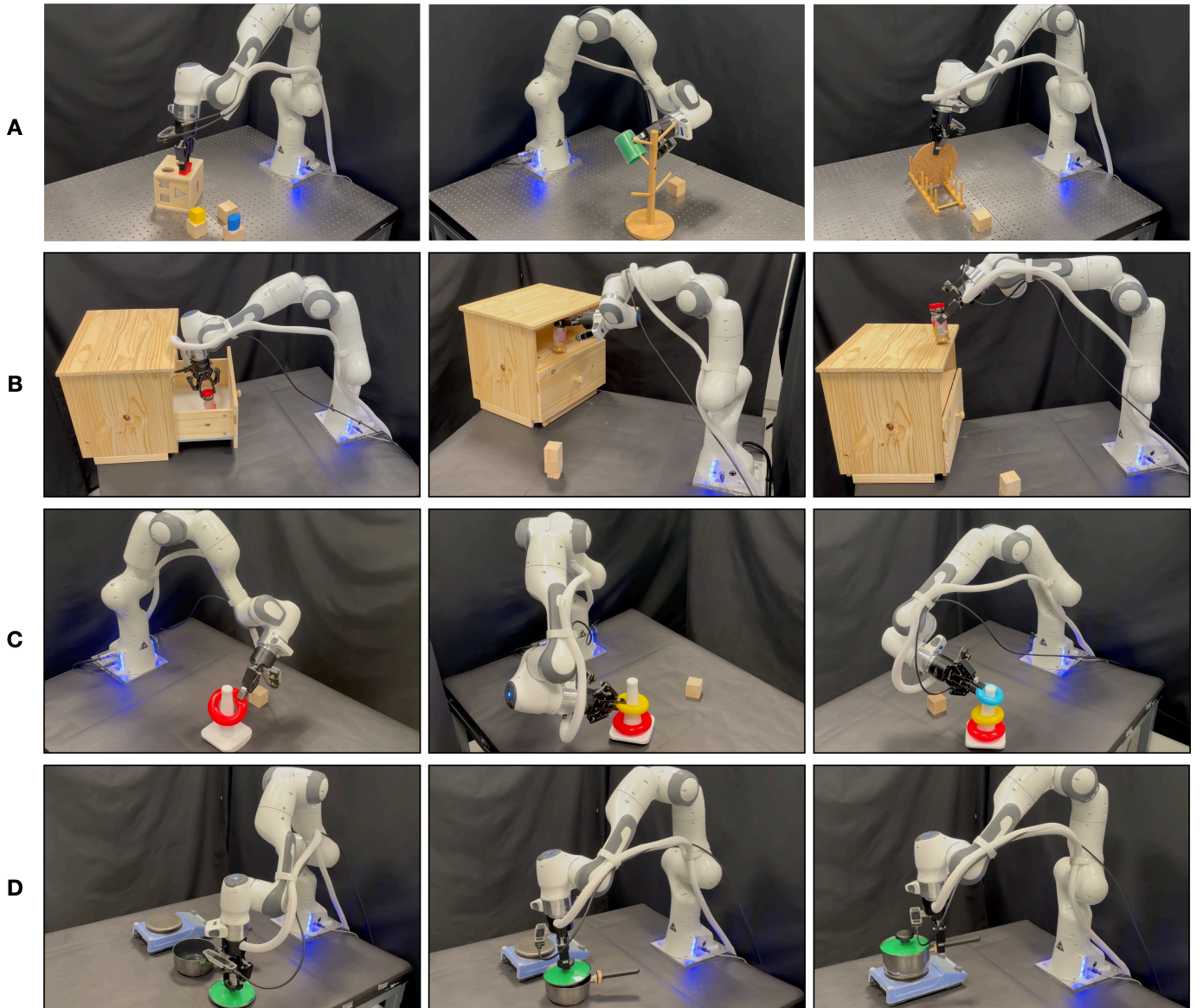


**Fig. 9: Robot performing various placement tasks in real-world environments.** In the real-world setting, with a simplified placement pipeline, the robot successfully executes a variety of placement tasks across a wide range of placement locations based on the prediction of the AnyPlace model. (A) We demonstrate peg-in-hole, cup-on-rack, and plate-on-rack tasks. (B) The robot places the bottle in different locations based on a language description. (C) The robot stacks rings of different radii. (D) The robot executes a long-horizon task where it places the lid on the pot and then places the pot on the stove.

to precisely place a lid on a pot before placing the pot on a stove. Our method ensures that placed objects are centered and properly aligned, highlighting its reliability in real-world tasks. To demonstrate the advantage of combining VLM-based placement location prediction and local placement pose prediction modules, we show that the robot is able to place a bottle at different locations on a shelf based on language descriptions, as shown in Figure 9 (B). The key advantage of AnyPlace lies in its ability to integrate VLM-based high-level placement prediction with local placement pose refinement. By focusing on local regions for placement prediction and leveraging a diverse synthetic training dataset, it allows

AnyPlace not only to generalize to real-world objects with significantly different geometries but also captures complex placement configurations with greater accuracy and flexibility.

## VI. LIMITATIONS

Our primary focus in this work is on predicting placement poses. However, challenges remain in executing the full pick-and-place task with the same level of generality. Not every stable grasp of an object can be used to place it at a specific pose, and performing rejection sampling in real-world scenarios can be both difficult and time-consuming. Nonetheless, we believe our synthetic dataset and evaluation pipeline provide a strong



foundation for advancing in this direction by enabling the generation of training data for an end-to-end pick-and-place model applicable to a wide range of real-world placement tasks.

While our approach improves precision in placement pose prediction, it is still limited by the accuracy of the point clouds it receives as input. Completing placement tasks that require high precision can be challenging with imperfect point cloud data. Recent advances in depth estimation from RGB images show promise in addressing this issue, as does continued progress in sensor quality. Another promising approach is implementing a policy that uses force/torque feedback to refine the final stage of placement. Similarly to the previous point, we believe our dataset and simulation pipeline provides a strong foundation for tackling this challenge by generating data for training reactive placement-execution policies.

The approach we propose does not include language conditioning in the low-level pose prediction model. As a result, we cannot distinguish between different types of placements at the same location. However, given the architecture of the low-level model, adding a language-conditioning input is straightforward. Our synthetic data generation pipeline is well-suited for this scenario, as it allows for the automatic addition of language conditioning to different placement types. Additionally, an LLM can be used to enhance diversity in language-conditioning data.

## VII. CONCLUSION

In this work, we presented a general pipeline for performing a wide range of object placement tasks using a robotic arm. We proposed a two-part framework consisting of a high-level module that determines potential placement locations and a low-level module that predicts fine placement poses. The core idea of our approach is to leverage a VLM to propose placement locations, allowing the low-level pose prediction model to focus only on the local region of interest in the object’s pointcloud. This effectively reduces complexity and enhances generalization. To train our model, we created a synthetic dataset containing thousands of randomly generated objects and placement poses. We demonstrated the effectiveness of the entire pipeline in both simulation and real-world experiments. In simulation, we showed that AnyPlace outperforms baseline methods in terms of success rate, coverage, and precision. We then validated its robustness and generalization in real-world settings, where, given a single RGB-D image, AnyPlace predicts diverse placement configurations in a zero-shot manner and successfully generalizes to unseen objects.

## ACKNOWLEDGMENTS

We would like to acknowledge the part of the funding provided by the University of Toronto’s Acceleration Consortium from the Canada First Research Excellence Fund, grant number CFREF-2022-00042. We would also like to thank Dr. Anders G. Frøseth, the Vector Institute, the Acceleration Consortium, Natural Resources Canada, and the Canada 150 Research Chairs program for their generous support.

## REFERENCES

- [1] Yun-Chun Chen, Haoda Li, Dylan Turpin, Alec Jacobson, and Animesh Garg. Neural shape mating: Self-supervised object assembly with adversarial shape priors. In *Proceedings of the IEEE/CVF Conference on Computer Vision and Pattern Recognition*, pages 12724–12733, 2022.
- [2] Cheng Chi, Siyuan Feng, Yilun Du, Zhenjia Xu, Eric Cousineau, Benjamin Burchfiel, and Shuran Song. Diffusion policy: Visuomotor policy learning via action diffusion. In *Proceedings of Robotics: Science and Systems (RSS)*, 2023.
- [3] Ethan Chun, Yilun Du, Anthony Simeonov, Tomas Lozano-Perez, and Leslie Kaelbling. Local neural descriptor fields: Locally conditioned object representations for manipulation. In *2023 IEEE International Conference on Robotics and Automation (ICRA)*, pages 1830–1836, 2023. doi: 10.1109/ICRA48891.2023.10160423.
- [4] Matt Deitke, Christopher Clark, Sangho Lee, Rohun Tripathi, Yue Yang, Jae Sung Park, Mohammadreza Salehi, Niklas Muennighoff, Kyle Lo, Luca Soldaini, Jiasen Lu, Taira Anderson, Erin Bransom, Kiana Ehsani, Huong Ngo, YenSung Chen, Ajay Patel, Mark Yatskar, Chris Callison-Burch, Andrew Head, Rose Hendrix, Favyn Bastani, Eli VanderBilt, Nathan Lambert, Yvonne Chou, Arnavi Chheda, Jenna Sparks, Sam Skjonsberg, Michael Schmitz, Aaron Sarnat, Byron Bischoff, Pete Walsh, Chris Newell, Piper Wolters, Tanmay Gupta, Kuo-Hao Zeng, Jon Borchardt, Dirk Groeneveld, Jen Dumas, Crystal Nam, Sophie Lebrecht, Caitlin Wittliff, Carissa Schoenick, Oscar Michel, Ranjay Krishna, Luca Weihs, Noah A. Smith, Hannaneh Hajishirzi, Ross Girshick, Ali Farhadi, and Aniruddha Kembhavi. Molmo and pixmo: Open weights and open data for state-of-the-art multimodal models, 2024. URL <https://arxiv.org/abs/2409.17146>.
- [5] Yufei Ding, Haoran Geng, Chaoyi Xu, Xiaomeng Fang, Jiazhaoh Zhang, Songlin Wei, Qiyu Dai, Zhizheng Zhang, and He Wang. Open6DOR: Benchmarking open-instruction 6-dof object rearrangement and a VLM-based approach. In *First Vision and Language for Autonomous Driving and Robotics Workshop*, 2024. URL <https://openreview.net/forum?id=RclUiexKMT>.
- [6] Ben Eisner, Yi Yang, Todor Davchev, Mel Vecerik, Jonathan Scholz, and David Held. Deep SE(3)-equivariant geometric reasoning for precise placement tasks. In *The Twelfth International Conference on Learning Representations*, 2024. URL <https://arxiv.org/abs/2404.13478>.
- [7] Hao-Shu Fang, Chenxi Wang, Hongjie Fang, Minghao Gou, Jirong Liu, Hengxu Yan, Wenhai Liu, Yichen Xie, and Cewu Lu. Anygrasp: Robust and efficient grasp perception in spatial and temporal domains. *IEEE Transactions on Robotics (T-RO)*, 2023.
- [8] Pete Florence, Corey Lynch, Andy Zeng, Oscar Ramirez,

- Ayzaan Wahid, Laura Downs, Adrian Wong, Johnny Lee, Igor Mordatch, and Jonathan Tompson. Implicit behavioral cloning. *Conference on Robot Learning (CoRL)*, 2021.
- [9] Chongkai Gao, Zhengrong Xue, Shuying Deng, Tianhai Liang, Siqi Yang, Lin Shao, and Huazhe Xu. Riemann: Near real-time se(3)-equivariant robot manipulation without point cloud segmentation. 2024.
- [10] Ankit Goyal, Jie Xu, Yijie Guo, Valts Blukis, Yu-Wei Chao, and Dieter Fox. Rvt: Robotic view transformer for 3d object manipulation. *arXiv:2306.14896*, 2023.
- [11] Ankit Goyal, Valts Blukis, Jie Xu, Yijie Guo, Yu-Wei Chao, and Dieter Fox. Rvt2: Learning precise manipulation from few demonstrations. *RSS*, 2024.
- [12] Zhanpeng He, Nikhil Chavan-Dafle, Jinwook Huh, Shuran Song, and Volkan Isler. Pick2place: Task-aware 6dof grasp estimation via object-centric perspective affordance. In *2023 IEEE International Conference on Robotics and Automation (ICRA)*, pages 7996–8002, 2023. doi: 10.1109/ICRA48891.2023.10160736.
- [13] Jonathan Ho, Ajay Jain, and Pieter Abbeel. Denoising diffusion probabilistic models. In *Proceedings of the 34th International Conference on Neural Information Processing Systems, NIPS '20*, Red Hook, NY, USA, 2020. Curran Associates Inc. ISBN 9781713829546.
- [14] Haojie Huang, Haotian Liu, Dian Wang, Robin Walters, and Robert Platt. Match policy: A simple pipeline from point cloud registration to manipulation policies, 2024. URL <https://arxiv.org/abs/2409.15517>.
- [15] Haojie Huang, Karl Schmeckpeper, Dian Wang, Ondrej Biza, Yaoyao Qian, Haotian Liu, Mingxi Jia, Robert Platt, and Robin Walters. Imagination policy: Using generative point cloud models for learning manipulation policies. *arXiv preprint arXiv:2406.11740*, 2024.
- [16] Stephen James, Kentaro Wada, Tristan Laidlow, and Andrew J. Davison. Coarse-to-fine q-attention: Efficient learning for visual robotic manipulation via discretisation, 2022. URL <https://arxiv.org/abs/2106.12534>.
- [17] Seungjae Lee, Yibin Wang, Haritheja Etukuru, H. Jin Kim, Nur Muhammad Mahi Shafiullah, and Lerrel Pinto. Behavior generation with latent actions. *arXiv preprint arXiv:2403.03181*, 2024.
- [18] Ilya Loshchilov and Frank Hutter. Decoupled weight decay regularization, 2019. URL <https://arxiv.org/abs/1711.05101>.
- [19] Mayank Mittal, Calvin Yu, Qinxu Yu, Jingzhou Liu, Nikita Rudin, David Hoeller, Jia Lin Yuan, Ritvik Singh, Yunrong Guo, Hammad Mazhar, Ajay Mandlekar, Buck Babich, Gavriel State, Marco Hutter, and Animesh Garg. Orbit: A unified simulation framework for interactive robot learning environments. *IEEE Robotics and Automation Letters*, 8(6):3740–3747, 2023. doi: 10.1109/LRA.2023.3270034.
- [20] Kieran A Murphy, Carlos Esteves, Varun Jampani, Srikanth Ramalingam, and Ameesh Makadia. Implicit-pdf: Non-parametric representation of probability distributions on the rotation manifold. In *Proceedings of the 38th International Conference on Machine Learning*, pages 7882–7893, 2021.
- [21] Chuer Pan, Brian Okorn, Harry Zhang, Ben Eisner, and David Held. TAX-pose: Task-specific cross-pose estimation for robot manipulation. In *6th Annual Conference on Robot Learning*, 2022. URL <https://arxiv.org/abs/2211.09325>.
- [22] Nikhila Ravi, Valentin Gabeur, Yuan-Ting Hu, Ronghang Hu, Chaitanya Ryali, Tengyu Ma, Haitham Khedr, Roman Rädle, Chloe Rolland, Laura Gustafson, et al. Sam 2: Segment anything in images and videos. *arXiv preprint arXiv:2408.00714*, 2024.
- [23] Hyunwoo Ryu, Hong in Lee, Jeong-Hoon Lee, and Jongeun Choi. Equivariant descriptor fields: Se(3)-equivariant energy-based models for end-to-end visual robotic manipulation learning, 2023. URL <https://arxiv.org/abs/2206.08321>.
- [24] Hyunwoo Ryu, Jiwoo Kim, Hyunseok An, Junwoo Chang, Joohwan Seo, Taehan Kim, Yubin Kim, Chaewon Hwang, Jongeun Choi, and Roberto Horowitz. Diffusion-edfs: Bi-equivariant denoising generative modeling on se(3) for visual robotic manipulation, 2023. URL <https://arxiv.org/abs/2309.02685>.
- [25] Nur Muhammad Mahi Shafiullah, Zichen Jeff Cui, Ariuntuya Altanzaya, and Lerrel Pinto. Behavior transformers: Cloning  $k$  modes with one stone, 2022. URL <https://arxiv.org/abs/2206.11251>.
- [26] Anthony Simeonov, Yilun Du, Andrea Tagliasacchi, Joshua B. Tenenbaum, Alberto Rodriguez, Pulkit Agrawal, and Vincent Sitzmann. Neural descriptor fields: Se(3)-equivariant object representations for manipulation, 2021. URL <https://arxiv.org/abs/2112.05124>.
- [27] Anthony Simeonov, Yilun Du, Yen-Chen Lin, Alberto Rodriguez Garcia, Leslie Pack Kaelbling, Tomás Lozano-Pérez, and Pulkit Agrawal. Se(3)-equivariant relational rearrangement with neural descriptor fields. In Karen Liu, Dana Kulic, and Jeff Ichnowski, editors, *Proceedings of The 6th Conference on Robot Learning*, volume 205 of *Proceedings of Machine Learning Research*, pages 835–846. PMLR, 14–18 Dec 2023. URL <https://proceedings.mlr.press/v205/simeonov23a.html>.
- [28] Anthony Simeonov, Ankit Goyal, Lucas Manuelli, Lin Yen-Chen, Alina Sarmiento, Alberto Rodriguez, Pulkit Agrawal, and Dieter Fox. Shelving, stacking, hanging: Relational pose diffusion for multi-modal rearrangement. *Conference on Robot Learning*, 2023.
- [29] Balakumar Sundaralingam, Siva Kumar Sastry Hari, Adam Fishman, Caelan Garrett, Karl Van Wyk, Valts Blukis, Alexander Millane, Helen Oleynikova, Ankur Handa, Fabio Ramos, Nathan Ratliff, and Dieter Fox. curobo: Parallelized collision-free minimum-jerk robot motion generation, 2023.
- [30] Aaron van den Oord, Oriol Vinyals, and Koray Kavukcuoglu. Neural discrete representation learning, 2018. URL <https://arxiv.org/abs/1711.00937>.

- [31] Ashish Vaswani, Noam Shazeer, Niki Parmar, Jakob Uszkoreit, Llion Jones, Aidan N. Gomez, Łukasz Kaiser, and Illia Polosukhin. Attention is all you need. In *Proceedings of the 31st International Conference on Neural Information Processing Systems, NIPS'17*, page 6000–6010, Red Hook, NY, USA, 2017. Curran Associates Inc. ISBN 9781510860964.
- [32] Yifan You, Lin Shao, Toki Migimatsu, and Jeannette Bohg. Omnihang: Learning to hang arbitrary objects using contact point correspondences and neural collision estimation. In *2021 IEEE International Conference on Robotics and Automation (ICRA)*. IEEE, 2021.
- [33] Wentao Yuan, Adithyavairavan Murali, Arsalan Mousavian, and Dieter Fox. M2t2: Multi-task masked transformer for object-centric pick and place. In *7th Annual Conference on Robot Learning*, 2023.

## APPENDIX

### A. Language Prompts for Molmo and Predicted Placement Visualization

In Figure 10 and Figure 11, we show additional language prompts used by the VLM to predict placement locations in both real-world and simulation experiments. Based on our observations, the Molmo VLM accurately identifies the correct placement locations in both real-world and simulated images based on the language input. Even when the predicted location is not perfectly centered, our low-level pose prediction model still works. For instance, when predicting the placement position of the bottle on the top shelf, the location may be at the edge. However, our model focuses on the local region centered at the proposed placement location and provides a pose that allows the robot to execute the task successfully.

### B. Additional Details on Model Training and Dataset

In Table IV, we list all the parameters used for training the AnyPlace low-level pose prediction models. Table V presents statistics on the number of placements generated using our synthetic dataset generation pipeline. Notably, by focusing only on the region of interest for placement pose prediction, AnyPlace models perform well across different placement tasks and generalize to unseen objects. They are trained with fewer than 2,000 samples per task, demonstrating the effectiveness of our design.

TABLE IV: Parameters for Model Training

Parameter	Value
Diffusion steps	5
Number of training iteration	500k
Batch size	48
Optimizer	AdamW [18]
Learning rate	$1 \times 10^{-4}$
Learning rate schedule	Linear warmup and cosine decay
Warmup epochs	50
Weight decay	0.1
Optimizer momentum	$\beta_1 = 0.9, \beta_2 = 0.95$

TABLE V: Dataset Size for Each Placement Task

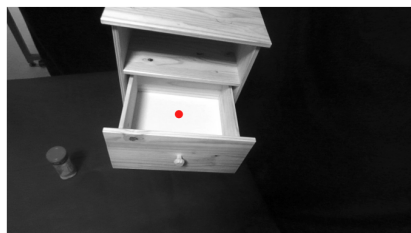
Placement Task	Number of Placements
Hanging	1,767
Stacking	1,696
Vial Insertion	1,107
Other Insertion	800

### C. Additional Details on Model Architecture

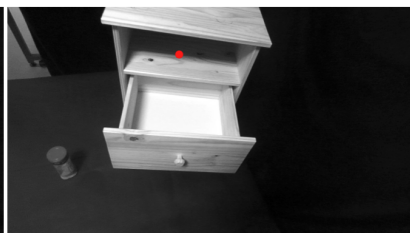
For our diffusion-based placement prediction model, we leverage a transformer architecture. We use self-attention layers to extract point cloud features for individual objects and cross-attention to learn joint features for placement pose prediction. Details of the model architecture are listed in Table VI.



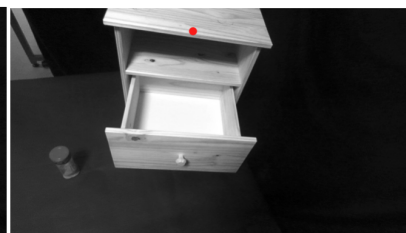
**Prompt:** "point to the base of the drawer where I can place the bottle"



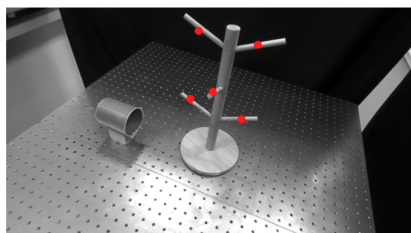
**Prompt:** "point to the middle layer where I can place the bottle"



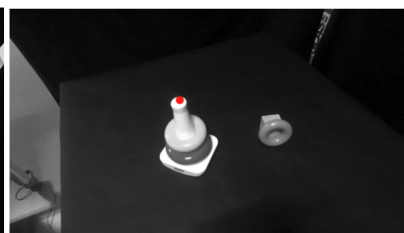
**Prompt:** "point to the top of the shelf where I can place the bottle"



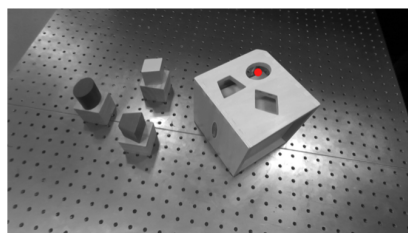
**Prompt:** "point to the tip of sticks on which I can hang a cup"



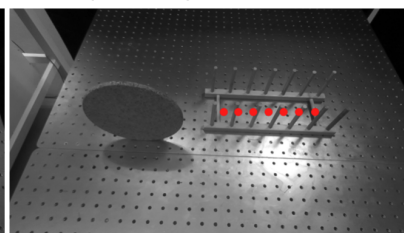
**Prompt:** "point to the tip of rack where I can place the ring"



**Prompt:** "point to the hole where i can place the circle"



**Prompt:** "point to empty slots in the middle of two poles on the rack where I can place the plate"



**Prompt:** "point to the pot where I can place the lid"



**Prompt:** "point to the top of the scale where I can place the pot"

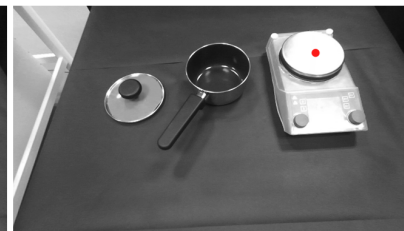


Fig. 10: Additional Language Prompts and VLM Output Visualization in the Real-World Evaluation.

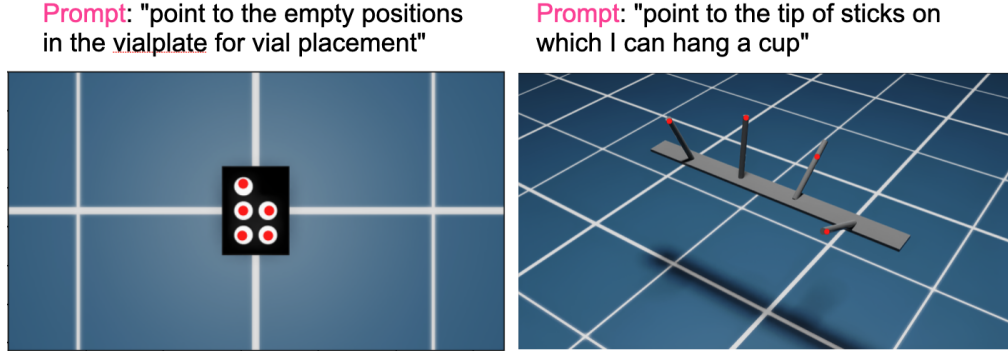


Fig. 11: **Language Prompts and VLM Output Visualization in the Simulation Evaluation.** In our simulation experiments, we use the VLM to generate placement locations on RGB images from the simulator. Based on this proposed location, we crop the point clouds and input them into our placement pose prediction model.

TABLE VI: Summary of Model Architecture

Model Component	Details
<b>Model Total Parameters</b>	4,279,688
<b>Number of Heads</b>	1
<b>Number of Self-attention Blocks</b>	4
<b>Number of Cross-attention Blocks</b>	4
<b>Point Cloud Feature Dimension</b>	258 (256 + one-hot embedding)
<b>Transformer Feature Dimension</b>	256
<b>Encoder</b>	
Self-Attention	Multi-Headed Attention (1 head)
Feedforward Layer	Linear (258 $\rightarrow$ 256), ReLU, Linear (256 $\rightarrow$ 258)
Normalization	LayerNorm
<b>Decoder</b>	
Self-Attention	Multi-Headed Attention (1 head)
Cross-Attention	Multi-Headed Attention (1 head)
Feedforward Layer	Linear (258 $\rightarrow$ 256), ReLU, Linear (256 $\rightarrow$ 258)
Normalization	LayerNorm